



A delay differential equation model for surface acoustic wave sensors

Z.C. Feng^{a,*}, Carmen Chicone^b

^aDepartment of Mechanical and Aerospace Engineering, University of Missouri-Columbia,
E2403B Engineering Building East, Columbia, MO 65211, USA

^bDepartment of Mathematics, University of Missouri-Columbia, Columbia, MO 65211, USA

Received 25 July 2002; received in revised form 20 January 2003; accepted 27 January 2003

Abstract

This paper presents a functional differential equation model for surface acoustic wave (SAW) devices. Closed-loop SAW delay line oscillators are modeled as differential equations with multiple delays. Stable oscillations of the circuit are associated with Hopf bifurcations. Conditions for Hopf bifurcations to occur are used to predict the mode number of the oscillator and its operating frequency. It is found that the operating frequency is close to the center frequency of the open-loop filter but is modulated by the effective separation distance between the generator and the receptor. The frequency relationship is applied to a tunable SAW oscillator to provide a phenomenological understanding of the mode jumping that is reported in experiments.

© 2003 Published by Elsevier Science B.V.

Keywords: Hopf bifurcations; Surface acoustic wave; Electric charge

1. Introduction

A surface acoustic wave (SAW) is an elastic wave, a Rayleigh wave [1], whose wave propagation energy is confined near a stress-free surface of a solid where it can be generated and detected with relative ease. SAW devices have found widespread use in sensors and in electronic components for telecommunications. Both of these applications take advantage of the time delay, i.e. the finite propagation time from the moment the wave is generated until it reaches a detector. In SAW sensors, small changes in the composition of the surface (such as the added mass by surface adsorption) cause changes in the wave propagation speed [2] that are detectable as changes of the time delay [3]. In SAW devices for telecommunications, surface acoustic waves are generated and received at multiple sources and detectors implemented by interdigital transducers. The signal follows electric to elastic and back to electric paths. Since the elastic path can be modified through geometric design [4–7], SAW devices with desired filter properties are easily constructed.

While the time delay is the essential variable responsible for SAW sensors, variations in wave propagation speeds are so small that changes in time delays are never measured

directly. Instead, a SAW device is configured to form a delay line oscillator [8–10] as in Fig. 1, where the interdigital transducer on the right (called the generator for convenience) converts an electric potential into surface elastic waves that are detected by the transducers on the left (called the receiver or receptor) and converted back to an electric signal. By amplifying this signal and applying it to the generator, we form a delay line closed loop. For an amplifier with an appropriate gain, the resulting delay line device will oscillate at a frequency that depends on the physical parameters. In other words, the closed loop converts variations in time delay to variations in oscillation frequency [11]. Since the frequency of a signal can be easily measured to an accuracy of one part per million [12], SAW sensors are extremely sensitive. For this reason, SAW sensors have found widespread applications as chemical sensors [13,14]. They also have many other potential applications, for instance, as immunoassays [15] and UV sensors [16].

In a delay line oscillator with delay-time τ and with electrical phase shift ϕ_E associated with the amplifiers and transmission lines, it is well-known [8,17–21] that if the loop gain exceeds unity, then oscillations occur at a frequency $\omega/2\pi$, such that

$$\omega\tau + \phi_E = 2\pi n \quad (1)$$

where n is an integer and $\omega\tau$ is the phase shift in the delay line. This relationship establishes the dependence of the

* Corresponding author. Tel.: +1-57-3884-4624; fax: +1-57-3884-5090.
E-mail address: fengf@missouri.edu (Z.C. Feng).

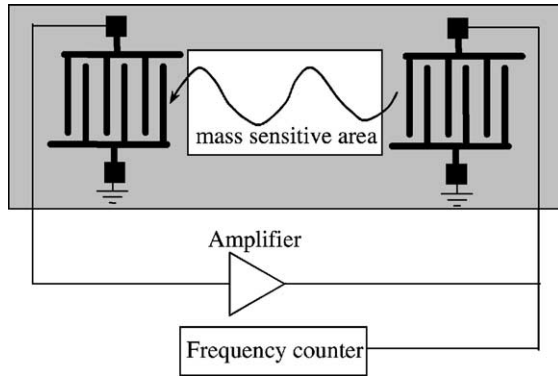


Fig. 1. A schematic diagram of a SAW sensor is depicted.

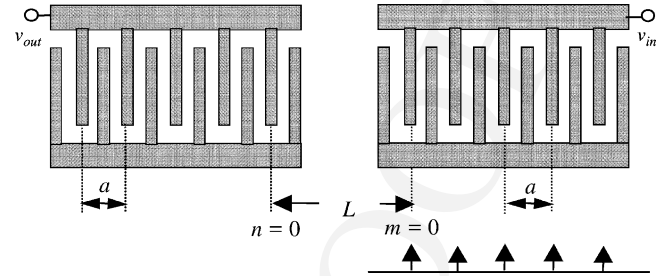


Fig. 2. A schematic model of the transducers is depicted. The vertical arrows represent the directions of the concentrated forces.

mechanical forces. In turn, these mechanical forces generate surface acoustic waves that are propagated throughout the solid substrate. Electrodes on the left sense the corresponding elastic waves by converting local strains into an electric charge or voltage.

We let M and N denote the number of force generators and receptors, respectively, and we make the following assumptions.

1. The elastic media is unbounded. In other words, we do not consider the reflections of the surface acoustic waves by the boundaries of the solid substrate. This approximation is reasonable since measures are taken in device design to eliminate reflections.
2. Following Hashimoto [7], we assume that a force proportional to the voltage is generated at each finger of the transducer on the right-hand side.
3. The displacement field felt by each finger of the transducer on the left-hand side is the superposition of the displacements caused by the concentrated forces at the generator.

Based on the above assumptions, the concentrated force at the m th finger is

$$f_m(t) = K_1 v_{in}(t) \tag{2}$$

where v_{in} is the input voltage for all fingers and K_1 is the proportionality constant of the transducer. We remark that detailed modeling of an electrode is very complicated. For example, in Matthews [4], the concentrated forces are applied at the edges of the electrode, and the directions of the forces are dependent on the polarity of the voltage. In this case, rather complicated algebra is required to obtain the transfer function.

Using superposition and the relation (A1) between a concentrated force applied at a distance and the corresponding displacement (which is derived in the Appendix A for the one-dimensional wave equation), the displacement u_n at the n th finger on the left is given by

$$\dot{u}_n(t) = \frac{1}{2V_R} \sum_{m=0}^{M-1} f_m \left(t - \frac{L + ma + na}{V_R} \right), \tag{3}$$

where V_R is the speed of the Rayleigh wave.

operating frequency on the delay time. Thus, it is adequate to use this relationship to compute the sensor frequency change in response to the change in the delay time. Because the integer n is arbitrary, the operating frequency of the delay line oscillator is not uniquely specified by the above relationship; rather, it is determined modulo an integer multiple of $2\pi/\tau$. Since the relationship between the time delay and the sensor geometry is not given, the equation above cannot explain experimental data on tunable magnetostatic surface-wave oscillators that show discontinuous jumps in operating frequency [18]. Although the operating frequency can be obtained experimentally, the ability to predict the operating frequency of a SAW device through modeling can greatly simplify the design and optimization processes. For more demanding applications of SAW devices, such as sensors for liquid phases [22–24], accurate modeling is essential.

In this work, we present a functional differential equation model for a delay line oscillator. By a linear stability analysis of the model equation, we obtain a criterion for the existence of a self-excited oscillation and use it to determine the corresponding unique operating frequency. We also examine the factors that affect this operating frequency.

In Section 2, we describe our model of the delay line oscillator. Its open-loop characteristics are studied in Section 3; its linear stability analysis is treated in Section 4. Section 5 gives a specific relationship between the operating frequency and the separation between the generator and the receptor. Section 6 applies the result in Section 4 to explain the mode jumping in tunable SAW oscillators. A generalization of the model is given in Section 7.

2. The mathematical model

The basic components that couple electrical energy to mechanical energy in the open-loop operation of the SAW delay line are depicted schematically in Fig. 2. In practice, the interdigital transducers are built on the surface of an elastic medium such as silicon. The structures on the right represent force generators that convert an electric voltage to

111
112
113
114
115
116
117
118
119
120
121
122
123
124
125
126
127
128
129
130
131
132
133
134
135
136
137
138
139
140
141
142
143
144
145
146
147
148
149
150
151
152
153

154 Let q_{out} denote the electric charge that is produced when
 155 the electrodes are subjected to the local strain. Since the
 156 strain at a point is proportional to the displacement gra-
 157 dient, which is in turn proportional to the displac-
 158 ement at that point, we assume that the charge is the sum
 159 of the charges produced at each finger and the charge from
 160 each finger is proportional to the displacement. Thus, we
 161 have

$$162 \quad q_{\text{out}}(t) = K_2 \sum_{n=0}^{N-1} u_n(t). \quad (4)$$

165 In the open loop, we assume that the output voltage is
 166 proportional to the charge, i.e.

$$167 \quad v_{\text{out}}(t) = K_3 q_{\text{out}}(t). \quad (5)$$

170 By combining the last two equations with Eq. (3), we obtain
 171 the relationship between the input and output voltages

$$172 \quad \dot{v}_{\text{out}}(t) = h \sum_{n=0}^{N-1} \sum_{m=0}^{M-1} v_{\text{in}} \left(t - \frac{L + ma + na}{V_R} \right), \quad (6)$$

175 where

$$176 \quad h = \frac{K_1 K_2 K_3}{2V_R} \quad (7)$$

179 3. The sinusoidal transfer function of the open loop

180 We let

$$181 \quad v_{\text{in}}(t) = \exp(j\omega t), \quad v_{\text{out}}(t) = G(\omega) \exp(j\omega t) \quad (8)$$

184 and substitute these expressions into Eq. (6) to obtain the
 185 sinusoidal transfer function

$$186 \quad G(\omega) = \frac{h}{\omega} \exp(-j\omega L) \sum_{m=0}^{M-1} \exp\left(-\frac{j\omega ma}{V_R}\right) \sum_{n=0}^{N-1} \exp\left(-\frac{j\omega na}{V_R}\right). \quad (9)$$

189 By evaluating the geometric series in (9), we have

$$190 \quad G(\omega) = \frac{h}{\omega} \exp(-j\omega L) \frac{1 - \exp(-j\omega Ma/V_R)}{1 - \exp(-j\omega a/V_R)} \\ \times \frac{1 - \exp(-j\omega Na/V_R)}{1 - \exp(-j\omega a/V_R)}, \quad (10)$$

193 and by using the identity

$$194 \quad \frac{1 - \exp(-j\omega Ma/V_R)}{1 - \exp(-j\omega a/V_R)} \\ = \frac{\exp(-j\omega Ma/2V_R)}{\exp(-j\omega a/2V_R)} \\ \times \frac{\exp[j\omega Ma/(2V_R)] - \exp[-j\omega Ma/2V_R]}{\exp[j\omega a/(2V_R)] - \exp[-j\omega a/2V_R]}, \quad (11)$$

the transfer function is expressed in the following more
 compact form:

$$G(\omega) = \frac{h}{\omega} \exp\left[-\frac{j\omega(L + (Ma + Na)/2 - a)}{V_R}\right] \\ \times \frac{\sin[\omega Ma/2V_R] \sin[\omega Na/2V_R]}{\sin[\omega a/2V_R] \sin[\omega a/2V_R]}. \quad (12)$$

The frequency response associated with the transfer func-
 tion G has the form of a band-pass filter with center
 frequency [3,7]

$$\omega_c = 2\pi \frac{V_R}{a}, \quad (13)$$

which is determined by the wave speed and the spacing
 parameter. We note that the separation distance L does not
 affect the center frequency. Thus, the center frequency of the
 open-loop device is not sensitive to adsorption on the sur-
 face. By substituting the definition of the center frequency
 into the frequency response function, we obtain the open-
 loop transfer function

$$G(\omega) = \frac{h}{\omega} \exp\left[-j\pi \left(\frac{2L}{a} + M + N - 2\right) \frac{\omega}{\omega_c}\right] g(\omega), \quad (14)$$

where

$$g(\omega) = \frac{\sin(\pi M \omega / \omega_c) \sin(\pi N \omega / \omega_c)}{\sin(\pi \omega / \omega_c) \sin(\pi \omega / \omega_c)}. \quad (15)$$

The function $G(\omega)$ is analogous to those obtained in [4,7,10].

The exponential term in the formula for G represents a
 phase lag. Also, the output–input amplitude ratio is propor-
 tional to $g(\omega)$. Since M and N are integers, g has a remov-
 able singularity at $\omega = \omega_c$, such that its extension, which we also
 denote by g , is continuous and bounded by MN . Fig. 3 shows
 the typical characteristics of the open-loop filter. Note that
 only signals whose frequencies are close to the center
 frequency are not drastically attenuated. As is well-known
 [4,7,10], the bandwidth and the side-lobe attenuation are
 dependent on the number of fingers M and N .

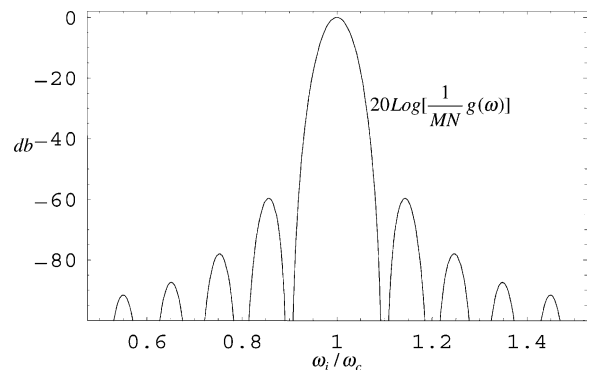


Fig. 3. For the case $M = 10$ and $N = 10$, the figure shows the logarithmic plot of $g(MN)$ vs. ω/ω_c .

233 **4. Stability analysis of the SAW delay line oscillator**

234 In closed-loop operation, the output signal of the receptor
235 is amplified and applied as an input to the generator. We will
236 ignore the delay in the amplifier and assume that

$$237 v_{in}(t) = Av_{out}(t) \quad (16)$$

238 where A is the amplifier gain. By substitution into Eq. (6), we
239 obtain the linear functional differential equation

$$240 \dot{v}_{in}(t) = Ah \sum_{n=0}^{N-1} \sum_{m=0}^{M-1} v_{in} \left(t - \frac{L + ma + na}{V_R} \right) \quad (17)$$

241 By setting $v_{in}(t) = e^{\lambda t}$ in Eq. (17), we find its characteristic
242 equation to be

$$243 \lambda = Ah \exp \left[-\frac{\lambda L}{V_R} \right] \sum_{n=0}^{N-1} \exp \left(-\frac{\lambda na}{V_R} \right) \sum_{m=0}^{M-1} \exp \left(-\frac{\lambda ma}{V_R} \right) \quad (18)$$

244 For $Ah > 0$, Eq. (18) can have a positive real root, and
245 therefore, the circuit can be unstable. In other words, the
246 voltage grows exponentially with time and saturates the
247 circuit. For the closed-loop circuit to sustain stable oscillation,
248 the instability must be avoided. Since no positive real
249 root is possible for $Ah > 0$, this can be accomplished using
250 negative feedback. We will assume from this point on that
251 negative feedback is used. It is possible, though, that this
252 instability may not arise even for positive feedback. For
253 instance, high pass filtering can be used to kill the dc gain. In
254 real circuits, typical transducers (such as PZTs) at the
255 receptor cannot maintain a constant output corresponding
256 to a constant strain. This property is analogous to a high pass
257 filter. In other words, this instability may be avoided in real
258 circuits without using either the negative feedback or an
259 additional high pass filter.

260 Assume that the instability due to a positive real characteristic
261 root is prevented by circuit design. Therefore, voltage disturbances
262 are attenuated if the feedback gain is small. On the other hand,
263 circuit oscillations will arise if the gain exceeds a threshold
264 value that corresponds to a Hopf bifurcation [25,26], where a
265 small amplitude oscillation arises from a change in the stability
266 of a steady state as some system parameter (the amplifier gain
267 in the present case) is changed. Since Hopf bifurcations occur
268 when a pair of complex conjugate roots of the characteristic
269 equation crosses the imaginary axis, the threshold values correspond
270 to amplifier gains for which the characteristic equation has a
271 pair of pure imaginary roots. Hence, to find the bifurcation
272 points, we substitute $\lambda = j\omega$ into the characteristic equation
273 and use the algebraic simplifications employed in the previous
274 section to obtain the equation

$$275 j\omega = Ah \exp \left[-j\pi \left(\frac{2L}{a} + M + N - 2 \right) \frac{\omega}{\omega_c} \right] \\ 276 \times \frac{\sin(\pi M\omega/\omega_c) \sin(\pi N\omega/\omega_c)}{\sin(\pi\omega/\omega_c) \sin(\pi\omega/\omega_c)}.$$

whose real part is equivalent to

$$277 \cos \left[\pi \left(\frac{2L}{a} + M + N - 2 \right) \frac{\omega}{\omega_c} \right] = 0. \quad (20)$$

Its solutions, the set of all

$$278 \omega_i = \frac{2i - 1}{2(2L/a + M + N - 2)} \omega_c, \quad (21)$$

279 such that i is a positive integer, are the frequencies of the
280 oscillations at the Hopf bifurcations; the corresponding
281 amplifier gains are

$$282 A_i = (-1)^i \frac{\omega_c \omega_i \sin(\pi\omega_i/\omega_c)}{h \omega_c \sin(\pi M\omega_i/\omega_c) \sin(\pi N\omega_i/\omega_c)}. \quad (22)$$

283 The index i is the mode number, and the gain A_i represents
284 the threshold for that particular mode to change stability.

285 **5. Operating frequency of the closed-loop oscillator**

286 In closed-loop operation, there is no oscillation if the gain
287 is zero. As the gain increases from zero and surpasses the
288 threshold value of a particular mode, that mode becomes
289 unstable. In a two-port acoustic-wave delay-line-based
290 oscillator loop, the gain is maintained so that only one mode
291 is excited. The selected mode has the lowest threshold value
292 and the corresponding frequency is the device operating
293 frequency.

294 Eqs. (21) and (22) can be used together to find the
295 operating frequency. To maintain stable oscillation, the
296 instability associated with the positive real characteristic
297 roots must be avoided. We assume that this is accomplished
298 through the use of negative feedback. For $Ah < 0$, Eq. (22)
299 shows that only the odd modes are unstable. Thus, the
300 possible mode numbers for negative feedback in Eq. (21)
301 are $i = 2j - 1$, where $j = 1, 2, 3, \dots$, and the corresponding
302 frequencies for these modes are

$$303 \omega_j = \frac{4j - 3}{2(2L/a + M + N - 2)} \omega_c. \quad (23)$$

304 Note that the average separation distance between the generator
305 and the receptor is

$$306 L_{av} = L + \frac{1}{2}(M - 1)a + \frac{1}{2}(N - 1)a, \quad (24)$$

307 and the average time delay is therefore

$$308 \tau_{av} = \frac{L_{av}}{V_R}. \quad (25)$$

309 Using Eqs. (23)–(25) and the definition of the center frequency
310 (13), we obtain the relation

$$311 \omega_j \tau_{av} = 2\pi j - \frac{3}{2}\pi, \quad \text{for } j = 1, 2, 3, \dots, \quad (26)$$

312 which is consistent with the result stated in Eq. (1). Our
313 model renders the delay time as the average delay between
314 the generator and the receptor.

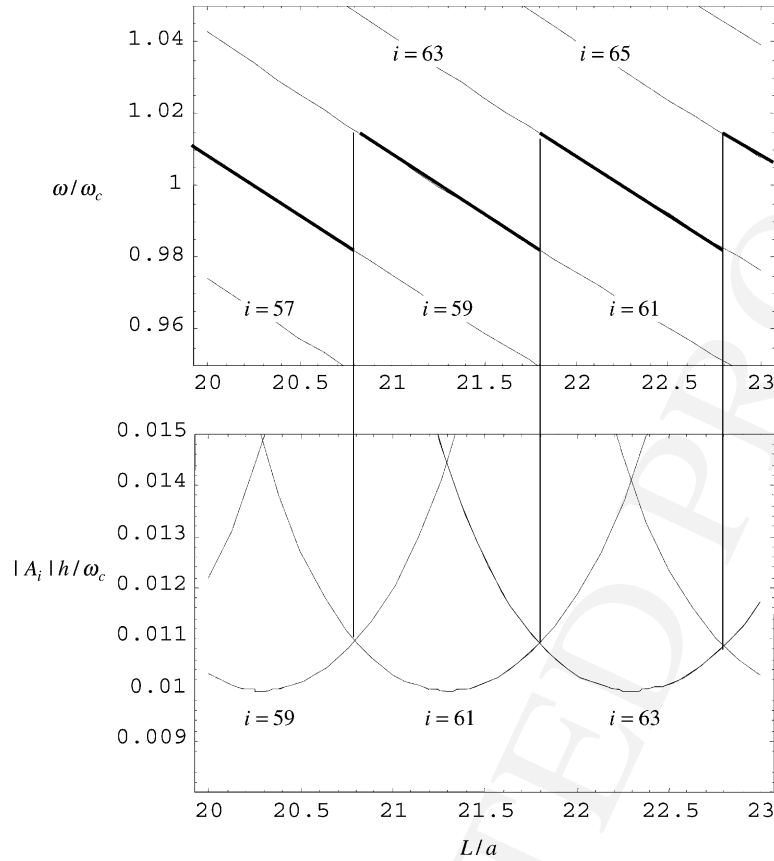


Fig. 4. The lower panel shows scaled gain vs. scaled separation. The upper panel shows scaled operating frequency vs. scaled separation for the closed-loop oscillator with $M = 10$ and $N = 10$.

339 In the following, we determine the oscillation frequency
 340 for the case $M = 10$ and $N = 10$. For each L/a (the dimensionless
 341 separation distance), there is a unique threshold
 342 amplifier gain, such that, for a small increase in its value,
 343 only one mode is unstable and all other modes are stable.
 344 Thus, the mode number and the frequency of the corresponding
 345 closed-loop oscillator are also functions of L/a .

346 Fig. 4 shows the relationship between the sensor operating
 347 frequency and the dimensionless separation distance. Note
 348 that the operating frequency, though it is dependent on the
 349 separation distance L , is close to the center frequency. Since
 350 the device is analogous to a band-pass filter in open-loop
 351 operation, the signal attenuation is smallest at the center
 352 frequency. In closed-loop operation, the operating frequency
 353 is dependent on the dimensionless separation distance.
 354 Nevertheless, the appropriate mode is selected so that the
 355 device operates near the center frequency. Recall that the
 356 center frequency is defined by the wave speed and the layout
 357 of the electrodes; thus, the approximate operating frequency
 358 of the sensor is also determined by the electrode layout.

359 Because of the open-loop characteristics shown in Fig. 3,
 360 once a separation distance is fixed, the mode whose frequency
 361 is closest to the open-loop center frequency requires
 362 the smallest amplifier gain to cause oscillations. This
 363 obvious fact is indicated in the lower panel in Fig. 4.

364 Furthermore, by Eq. (21), if the dimensionless separation
 365 L/a is large, then only modes with high mode numbers will
 366 have frequencies close to ω_c .

367 In typical SAW sensors, the separation between the
 368 generator and the receptor is fixed. When additional mass
 369 is adsorbed by the sensor surface, the wave speed is reduced.
 370 This results in an increased time delay between the generator
 371 and the receptor. In other words, the effective separation
 372 distance between the generator and the receptor is modified
 373 by the surface adsorption.

374 As illustrated in Fig. 4, the sensor operation may jump
 375 from one mode to another as the effective dimensionless
 376 separation distance L/a changes. To avoid the uncertainty
 377 that might arise from mode jumping, the sensor should be
 378 designed to operate at a fixed mode number; that is, the
 379 sensor measurement range must not exceed the interval
 380 defined by the corresponding continuous linear segment.
 381 The lower panel in Fig. 4 shows that the measurement range
 382 is approximately the frequency jump between neighboring
 383 modes. Using Eq. (23), this frequency jump is

$$384 \Delta\omega = \omega_j - \omega_{j-1} = \frac{4}{2(2L/a + M + N - 2)} \omega_c. \quad 386$$

387 Therefore, the measurement range decreases as the separation
 388 distance increases.

389 In SAW sensors, fabrication tolerances make it difficult to
 390 avoid mode jumping. But, by applying a phase shift adjust-
 391 ment to the amplified electrical signal, it is possible to tune
 392 the frequency by changing the time delay ([10], p. 369),
 393 which is equivalent to changing the effective separation
 394 distance L .

395 Our linear model predicts that for an amplifier gain above
 396 the threshold value, the corresponding mode is unstable and
 397 the circuit will oscillate with exponentially growing ampli-
 398 tude. In actual SAW sensors, a variable attenuator controls
 399 the oscillation amplitude ([10], p. 369). The amplifier and
 400 the variable attenuator are nonlinear circuit elements that
 401 affect the output signal $v_{out}(t)$. A cubic law has been
 402 proposed in [19] to represent these nonlinear elements.
 403 For devices operating at high frequencies, the circuit
 404 dynamics must be included in the model. Thus (functional)
 405 differential equations are required to accurately model the
 406 circuit, which includes the amplifier and the variable
 407 attenuator.

408 **6. Mode jumping in tunable surface-wave**
 409 **oscillators**

410 By inspection of Fig. 4, we note that the operating
 411 frequency of the SAW device is a discontinuous function
 412 of the separation distance L . The operating frequency varies
 413 with the separation distance but remains close to the center
 414 frequency of the open loop by mode jumping.

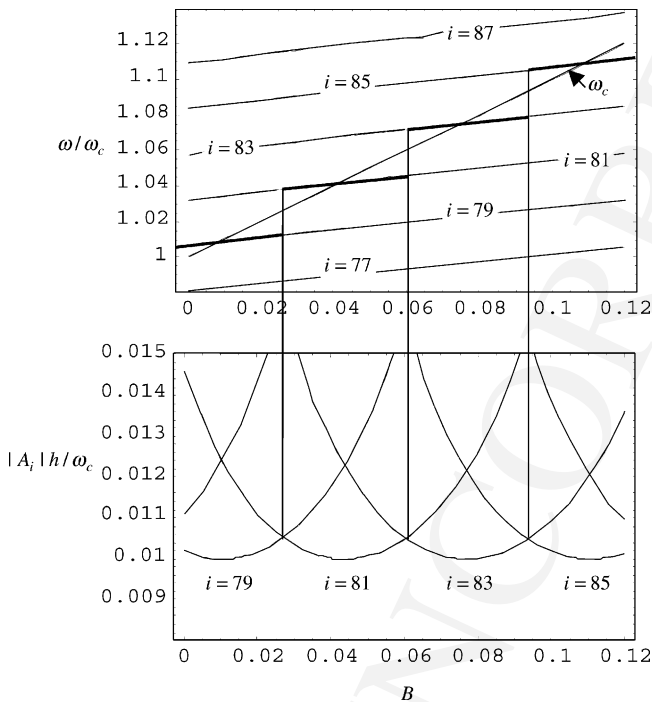


Fig. 5. For $M = 10$ and $N = 10$, the lower panel depicts the amplitude threshold vs. the magnetic field strength, and the upper panel depicts the corresponding operating frequency.

The center frequency of the sensor can be tuned by
 applying an external field, for instance a magnetic field
 [18]. Mode jumping, due to changes in the center frequency,
 has been observed in experiments with SAW oscillators [18].
 Our delay equation model can be used to explain this
 phenomenon.

In the absence of a detailed model for the magnetostatic
 surface-wave oscillator, we assume that the parameter B is
 proportional to the strength of the magnetic field and let the
 relations $\omega_c = \omega_0(1 + B)$ and $L/a = 30(1 + B)$ account for
 the effect of the magnetic field on the center frequency and
 on the dimensionless separation. For the case $M = 10$ and
 $N = 10$, the amplitude threshold and the corresponding
 operating frequency are shown in Fig. 5. We again assume
 that negative feedback is used and the circuit oscillates in
 odd modes. Note that the operating frequency is approxi-
 mately a linear function of the field strength, but discontin-
 uous jumps in frequency occur as the field strength changes
 continuously. This phenomenon is exactly what was
 observed in the experiment [18].

415 **7. Generalization to account for actuator and**
 416 **amplifier dynamics**

Several of our simplifying assumptions can be relaxed to
 make models that more accurately represent the properties
 of real circuits. To account for the dynamics of the actuators
 and the amplifier, the voltages $v_{in}(t)$ and $v_{out}(t)$ can be
 related by a linear differential equation, instead of Eq. (16).
 The most general form of this equation,

$$a_n \frac{d^n v_{in}(t)}{dt^n} + a_{n-1} \frac{d^{n-1} v_{in}(t)}{dt^{n-1}} + \dots + a_0 v_{in}(t) = b_m \frac{d^m v_{out}(t)}{dt^m} + b_{m-1} \frac{d^{m-1} v_{out}(t)}{dt^{m-1}} + \dots + b_0 v_{out}(t), \quad (27)$$

can be combined with Eq. (6) to obtain a model for the
 closed-loop system. By taking the Fourier transform of
 Eq. (27), we obtain the sinusoidal relationship

$$v_{in}(t) = A(\omega) \exp[-j\phi(\omega)] v_{out}(t). \quad (28)$$

For $v_{out}(t) = \exp(j\omega t)$, the amplitude and phase functions
 $A(\omega)$ and $\phi(\omega)$ (where a positive $\phi(\omega)$ represents a phase
 lag) are determined by the coefficients of the differential
 equation; in fact, we find that

$$A(\omega) \exp[-j\phi(\omega)] = \frac{b_m(j\omega)^m + b_{m-1}(j\omega)^{m-1} + \dots + b_0}{a_n(j\omega)^n + a_{n-1}(j\omega)^{n-1} + \dots + a_0}. \quad (29)$$

If $v_{in}(t) = \exp(j\omega t)$, then

$$\dot{v}_{in}(t) = j\omega v_{in}(t) \quad (30)$$

463 and the criterion for oscillations obtained by combining
464 (24), (26), and (6) is

$$465 \quad j\omega = A(\omega)h \exp \left[-j\pi \left(\frac{2L}{a} + M + N - 2 \right) \frac{\omega}{\omega_c} - j\phi(\omega) \right] \\ \times \frac{\sin(\pi M\omega/\omega_c) \sin(\pi N\omega/\omega_c)}{\sin(\pi\omega/\omega_c) \sin(\pi\omega/\omega_c)}. \quad (31)$$

467 Assuming that negative feedback is used and employing the
468 same procedures as in Section 5, we obtain the relationship

$$470 \quad \omega_j \tau_{av} + \phi(\omega_j) = 2\pi j - \frac{3}{2}\pi, \quad (32)$$

473 which is again in agreement with Eq. (1).

474 8. Conclusion

475 A functional differential equation model for a delay-line
476 oscillator SAW device is proposed. Based on this model, it is
477 found that the operating frequency is close to the center
478 frequency of the open loop and is modulated by the separa-
479 tion between the generator and the receptor. This depen-
480 dence is the fundamental mechanism for SAW sensors. The
481 model also accounts for the mode jumping that is observed
482 in tunable surface wave oscillators.

483 Acknowledgements

484 This research is supported by a grant to Z.C.F. from
485 National Science Foundation (CMS0115828) and a grant
486 to C.C. from the research board of the University of Missouri.

487 Appendix A

488 Consider the one-dimensional wave equation in the form

$$489 \quad \frac{\partial^2 U}{\partial t^2} = c^2 \frac{\partial^2 U}{\partial x^2} + F(x, t),$$

491 where U is a displacement, c the wave speed, and F the force
492 per density; that is, the function F has gcs units cm/s^2 . A
493 particular solution u of the wave equation with zero initial
494 data is given by

$$495 \quad U(x, t) = \frac{1}{2c} \int_0^t \int_{x-c(t-s)}^{x+c(t-s)} F(y, s) dy ds.$$

499 For the case of a concentrated force per density at position
500 $x = \xi$ given by

$$501 \quad F(x, t) = \delta(x - \xi)f(t),$$

504 where δ is the unit impulse function at $x = 0$, let us note that
505 $\delta(x - \xi)$ has units of inverse length, $f(t)$ has units $(\text{cm/s})^2$, and

$$506 \quad u(t) := U(0, t) = \frac{1}{2c} \int_0^t f(s) \left(\int_{-c(t-s)}^{c(t-s)} \delta(y - \xi) dy \right) ds$$

$$= \frac{1}{2c} \int_0^t f(s) \left(\int_{\xi-c(t-s)}^{\xi+c(t-s)} \delta(y) dy \right) ds \\ = \frac{1}{2c} \int_0^t f(s) (1 - V_{t-\xi/c}(s)) ds,$$

511 where $V_b(s)$ is the unit step function (whose value is zero for
512 $s < b$ and one for $s \geq b$). By evaluating the last integral, we
513 have that $u(t) = 0$ for $t < \xi/c$ and

$$514 \quad u(t) = \frac{1}{2c} \int_0^{t-\xi/c} f(s) ds$$

515 for $t \geq \xi/c$. Hence for $t \geq \xi/c$,

$$516 \quad \dot{u}(t) = \frac{1}{2c} f\left(t - \frac{\xi}{c}\right) \quad (A.1)$$

517 Finally, we note that the units on both sides of this equation
518 are cm/s .

References

- 519 [1] Y.C. Fung, Foundations of Solid Mechanics, Prentice-Hall, Engle-
520 wood Cliffs, NJ, 1965, pp. 178–181.
- 521 [2] B.A. Auld, Acoustic Fields and Waves in Solids, vol. 2, Wiley, New
522 York, 1973.
- 523 [3] A. D'Amico, E. Verona, SAW sensors, Sens. Actuators 17 (1989)
524 55–66.
- 525 [4] H. Matthews, Surface Wave Filters: Design, Construction, and Use,
526 Wiley, New York, 1977.
- 527 [5] D.P. Morgan, Surface-Wave Devices for Signal Processing, Elsevier,
528 Amsterdam, 1985.
- 529 [6] S. Datta, Surface Acoustic Wave Devices, Prentice-Hall, Englewood
530 Cliffs, NJ, 1986.
- 531 [7] K. Hashimoto, Surface Acoustic Wave Devices in Telecommunica-
532 tions: Modeling and Simulation, Springer, New York, 2000.
- 533 [8] E.A. Ash, Fundamentals of signal processing devices, topics in
534 applied physics, in: A.A. Oliner (ed.) Acoustic Surface Waves, vol.
535 24, Springer, New York, 1978, pp. 97–185.
- 536 [9] H. Wohltjen, R. Dessy, Surface acoustic wave probe for chemical
537 analysis, Anal. Chem. 51 (1979) 1458–1475.
- 538 [10] D.S. Ballantine, R.M. White, S.J. Martin, A.J. Ricco, E.T. Zellers,
539 G.C. Frye, H. Wohltjen, Acoustic Wave Sensors: Theory, Design,
540 and Physico-Chemical Applications, Academic Press, San Diego,
541 1997.
- 542 [11] H. Wohltjen, Mechanism of operation and design considerations for
543 surface acoustic wave device vapour sensors, Sens. Actuators 5
544 (1984) 307–325.
- 545 [12] W.H. King, Piezoelectric sorption sensor, Anal. Chem. 36 (9) (1964)
546 1735–1739.
- 547 [13] S.L. Rose-Pehrsson, J.W. Grate, D.S. Ballantine, P.C. Jurs, Detection
548 of hazardous vapors including mixtures using pattern recognition
549 analysis of responses from surface acoustic wave devices, Anal.
550 Chem. 60 (1988) 2801–2811.
- 551 [14] J.W. Grate, A. Snow, D.S. Ballantine, H. Wohltjen, M.H. Abraham,
552 R.A. McGill, P. Sasson, Determination of partition coefficients from
553 surface acoustic wave vapor sensor responses and correlation with
554 gas-liquid chromatographic partition coefficients, Anal. Chem. 60
555 (1988) 869–875.
- 556 [15] J. Roederer, G.J. Bastiaans, Microgravimetric immunoassay with
557 piezoelectric crystals, Anal. Chem. 55 (1983) 2333–2336.

- 564 [16] D. Ciplys, R. Rimeika, A. Sereika, R. Gaska, M.S. Shur, J.W. Yang, 586
 565 M.A. Khan, GaN-based SAW delay line oscillator, *Electron. Lett.* 37 587
 566 (2001) 545–546. 588
- 567 [17] M.F. Lewis, Surface acoustic wave devices and applications. Part 6. 589
 568 Oscillators-the next successful surface acoustic wave device? 590
 569 *Ultrasonics* 12 (1974) 115–123. 591
- 570 [18] N. Miller, D. Brown, Tunable magnetostatic surface wave oscillator, 592
 571 *Electron. Lett.* 12 (1976) 209–210. 593
- 572 [19] A. Lantz, J. Salset, Mode analysis of a SAW delay line oscillator, 594
 573 *IEEE Trans. Sonics Ultrason.* SU-27 (1980) 266–271. 595
- 574 [20] W. Ishak, 4–20 GHz magnetostatic-wave delay line oscillator, 596
 575 *Electron. Lett.* 19 (1983) 930–931. 597
- 576 [21] S.N. Dunaev, Y.K. Fetisov, Multimode oscillation and mode locking 598
 577 of magnetostatic wave delay line oscillator, *Electron. Lett.* 28 (1992) 599
 578 789–791. 600
- 579 [22] M. Thompson, G.L. Hayward, Mass response of the thickness-shear 601
 580 mode acoustic wave sensor in liquids as a central misleading dogma, 602
 581 in: *Proceedings of the 1997 IEEE International Frequency Control 603*
 582 Symposium, 1997, pp. 114–119. 604
- 583 [23] S. Shiokawa, J. Kondoh, Surface acoustic wave sensor for liquid- 605
 584 phase application, in: *Proceedings of the 1997 IEEE Ultrasonics 606*
 585 Symposium, 1999, pp. 445–452. 607
- 603
- [24] T. Nomura, A. Saitoh, Y. Horikoshi, S. Furukawa, Liquid sensing 586
 system based on two port SH-SAW resonator, in: *Proceedings of the 587*
 1997 IEEE Ultrasonics Symposium, 1999, pp. 477–480. 588
- [25] J.K. Hale, S.M. Verduyn Lunel, *Introduction to Functional 589*
 Differential Equations, Springer, New York, 1993, pp. 331–335. 590
- [26] O. Diekmann, S.A. van Gils, S.M. Verduyn Lunel, H.-O. Walther, 591
 Delay Equations: Functional-, Complex-, and Nonlinear Analysis, 592
 Springer, New York, 1995, pp. 287–301. 593

Biographies

Z.C. Feng earned his PhD degree in mechanics from the University of 595
 Minnesota. He is currently, on the faculty of the University of Missouri- 596
 Columbia. His research interests are microelectromechanical systems and 597
 nonlinear dynamics. 598

C. Chicone earned his PhD in mathematics from the University of 599
 Wisconsin in 1977. He is a Professor of Mathematics at the University of 600
 Missouri-Columbia. His research interests include applied mathematics 601
 and dynamical systems. 602